SUPPLEMENTARY INFORMATION

White light scattering

In order to extract the plasmon linewidth we measured the scattering spectra of individual gold nanorods. For this purpose a dilute solution of gold nanorods (average size 90×30 nm) in 1% polyvinyl alcholol (PVA) was spincoated onto a glass coverslip. To locate the nanorods in our optical setup we imaged the sample surface using single-particle white-light scattering spectroscopy.[1,2] The reflected light from a spatially filtered quartz tungsten halogen lamp was collected by the focusing objective (1.4 NA oil immersed) and directed to a photo multiplier tube (PMT, Oriel Instruments). The spot was raster-scanned over the sample surface. To increase the visibility of the rods, the reflected light was bandpass-filtered before detection. Some nanorods appear dimmer because part of their scattering spectrum falls outside the filter band. The unfiltered scattering spectrum of each individual nanorod was dispersed by a spectrograph on a charge coupled device.

In Fig. 1a we show a raster scan of the sample surface. Diffraction limited spots indicate the location of isolated single gold nanorods. In Fig. 1b we show a selection of white light scattering spectra of individual gold nanorods. The scattering spectra are background corrected and normalized to the spectral profile of the light source. The spectra exhibit a strong longitudinal plasmon resonance between 1.5 and 1.7 eV. The difference in scattered intensity is caused by differences in particle volume. From Lorentzian fits we obtained an average linewidth of 107±15 meV, which is in good agreement with earlier reports on similar sized gold nanorods.[3] Although the gold nanorods used in our optical recording medium are smaller, the single particle linewidth is not expected to differ by more than 20–30%.[3]

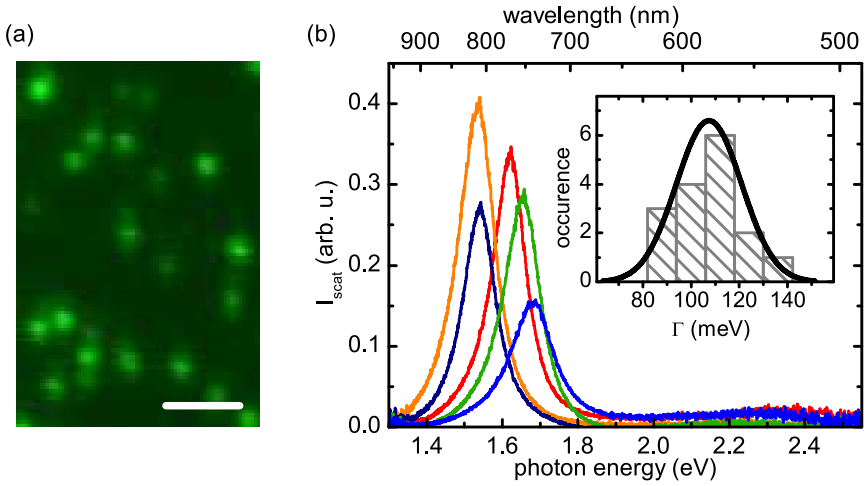

Figure 1: **White light scattering spectroscopy** (a) White light raster scan of the sample surface showing diffraction limited spots indicating the location of isolated single gold nanorods. Bar length 2 μm. (b) Scattering spectrum of five individual gold nanorods in unpolarized white light. The inset shows statistics of the extracted Lorentzian linewidths.

Polarization dependent bleaching of the extinction

We performed transmission spectroscopy of individual recorded pixels to characterize the polarization dependent bleaching in the extinction profile. The sample consisted of a spin coated layer of gold nanorods doped in PVA. The sample thickness was measured with an atomic force microscope, and was found to be ≈ 1 μm. The normalized extinction profiles of the as-prepared aqueous nanorod solutions are shown in Fig. 2, together with the extinction profile of the spin coated PVA film. The slight red-shift of the longitudinal surface plasmon peak is caused by the higher dielectric constant of PVA compared to water.

For the white light transmission spectroscopy, the spatially filtered output from a quartz tungsten halogen light source was focused onto the sample through a 0.95 NA objective lens, and collected in transmission by a condenser. The transmitted light was dispersed on a charge coupled device by a spectrograph. The transmission of the film in an unrecorded region was taken as the background. An electro-optic modulator (ConOptics Inc) was used to pick a single pulse from the 82 MHz pulse train of a titanium sapphire laser source for recording. A pixel was recorded using a linear polarization.

In Fig. 2b we show the change in extinction caused by the recording laser pulse. A bleaching occurred in the extinction spectrum centered around the recording laser wavelength (indicated by the arrows in Fig. 2b). As we show in the inset, the polarized transmission profile followed a dipolar angle dependence. This effect is due to the interaction of the linear laser light polarization with the dipolar surface plasmon resonance of the gold nanorods, which only selectively reshapes the nanorods which are on resonance with the laser light.

In Fig. 2 in the main text we directly verified this orientation and aspect ratio dependent reshaping by imaging the rods in a scanning electron microscope (SEM), before and after irradiation. It proved difficult to acquire well-focused images when the rods were doped in a 200 nm PVA matrix, mainly because the long aspect ratio rods rods we employed only have a radius of ~ 2.5 nm. We therefore embedded the nanorods in an extremely thin PVA film (< 20 nm thick),

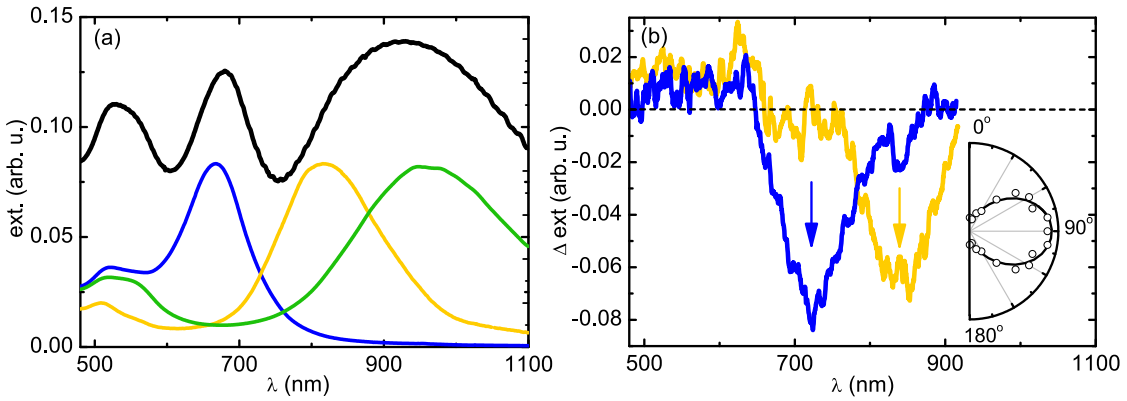

Figure 2: **Transmission spectroscopy of recorded pixels**(a) Large area extinction profile of PVA doped with the three distributions of gold nanorods, measured with unpolarized white light. The bottom spectra show the extinction profiles of the three individual batches of aqueous gold nanorods. (b) Change in extinction after irradiation with a linear polarized, single femtosecond laser pulse of 710 nm (dark blue line) and 840 nm (light yellow line). The spectrum was measured on a single recorded pixel by illuminating with tightly focused, linearly polarized white light. The inset shows the polarization dependent extinction modulation, with a dipolar cosine fit (solid line).

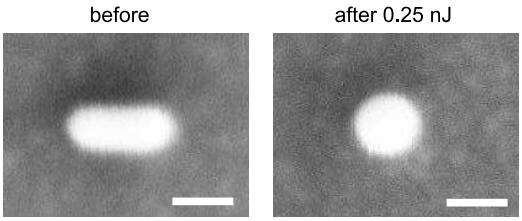

Figure 3: **SEM before and after irradiation** Scanning electron micrographs before and after irradiation of a nanorod embedded in a 200 nm PVA film. The nanorod was irradiated with a pulse energy of 0.25 nJ at the longitudinal surface plasmon peak of 750 nm with a polarization aligned to the long particle axis. Bar length 50 nm.

of which the results are presented in the main text. However, the very thin PVA film did not retain the nanorods, and we observed lift-off upon irradiation.

To verify that this lift-off does not occur when the rods are embedded in a thicker PVA film, we repeated this experiment with nanorods embedded in a 200 nm PVA matrix. The nanorods we employed here were significantly larger (average size 90×30 nm), allowing us to acquire SEM images. In Fig. 3 we show SEM images before and after irradiation of a large nanorod. The rod was irradiated with a single femtosecond laser pulse tuned on resonance with the longitudinal surface plasmon peak at 750 nm. We repeated this experiment for ≈ 80 nanorods embedded in PVA, none of which lifted off the substrate upon irradiation. Because the films we employed for optical recording are much thicker (~ 1 μm) than the films employed here, lift-off does not occur in the recording medium.

Estimation of particle temperature

The laser induced reshaping of the nanorods occurs when the particle temperature exceeds the melting temperature. We will estimate the maximum rise in lattice temperature by employing simple thermodynamic considerations. The amount of energy absorbed by a nanorod can be expressed as $Q = \sigma_{abs} I$, where σ_{abs} is the absorption cross section of the nanorod at the laser wavelength, and I is the laser pulse energy density in the focal plane. Typical values in our experiments are $\sigma_{abs} \sim 7 \times 10^{-15}$ m^2 (see for example Muskens *et al.*,[4] who measured σ_{abs} for nanorods with a size similar to the ones we used) and $I = 200$ Jm^{-2}. We then find $Q = 1.4$ pJ for a nanorod with a longitudinal SPR on resonance with the laser light. The temperature rise ΔT in a nanorod can then be expressed as

$$\Delta T = \frac{Q - m\Delta H}{m c_p}, \tag{1}$$

with m the mass of the nanorod (typical value 9×10^{-20} kg for a 45 × 12 nm rod), ΔH the heat of fusion of gold (6.5×10^4 Jkg^{-1}), and c_p the specific heat capacity of gold (129 Jkg^{-1}K^{-1}). This gives us an estimated increase in lattice temperature of ΔT$\sim 10^5$ K.

However, this temperature is unrealistically high due to the effect of absorption saturation, which we have ignored in this analysis. In a previous report on small gold nanospheres[5] it was found that absorption saturation occurs at laser energy densities of 10^{12} Wcm^{-2}. In our case the equivalent laser energy density is of the order of 10^{15} Wcm^{-2} (assuming 200 Jm^{-2} and a pulse duration of 100 fs), which is far above the estimated energy density at which absorption saturation is expected. We therefore expect the temperature in the nanorods to be significantly lower than we estimated here, but still well above the melting point of gold ($T_{melt} = 1337$ K).

Two-photon photoluminescence of single gold nanorods

TPL characteristics

Here we present a comprehensive study on the general characteristics of two-photon induced luminescence (TPL) in single gold nanorods. For this purpose we spin coated a dilute solution of gold nanorods (average size 90×30 nm) in a 1% PVA solution onto a glass coverslip. The TPL was excited and collected by the same 0.95 NA objective lens. The TPL signal was detected by a PMT (Hamamatsu H7422-40P).

In Fig. 4a we show a raster scan of the sample surface where diffraction limited spots indicate the location of well separated gold nanorods. To confirm the two-photon character of the luminescence excitation we increased the average excitation power from 50–120 μW and monitored the TPL intensity integrated over the whole spot in the raster scan. The slope of the linear fit in Fig. 4b is 1.94, which confirms the two-photon character of the excitation.

In Fig. 4c we present additional data to complement the TPL curves shown in Fig. 3 in the main text. We show the TPL excitation profiles for four more individual gold nanorods. The

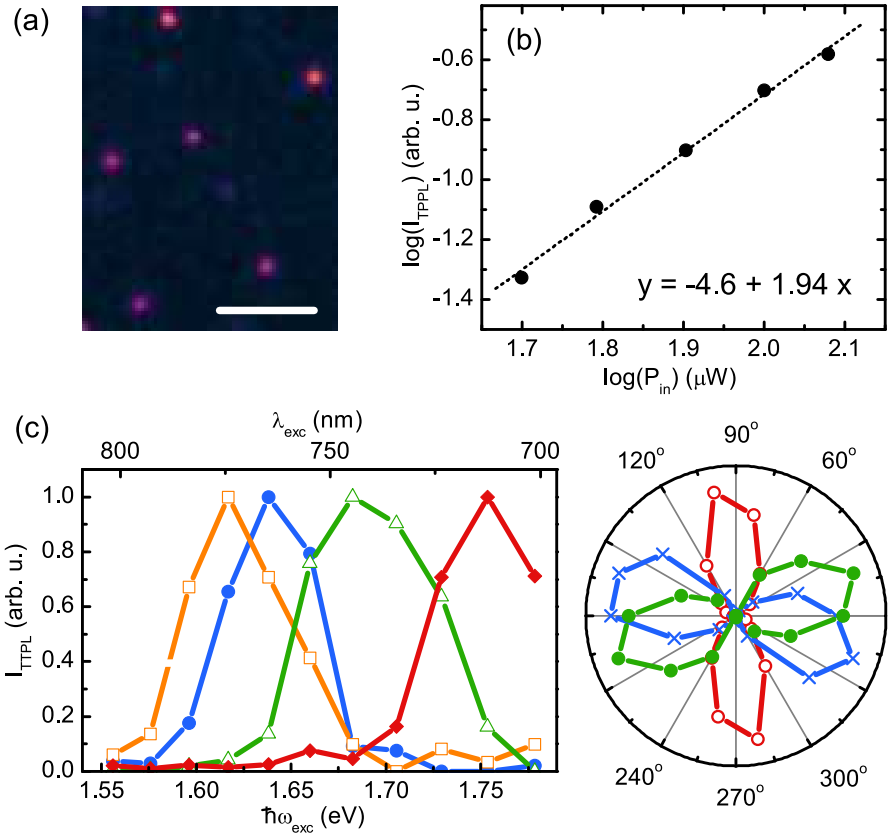

Figure 4: **Two-photon luminescence (TPL) of single gold nanorods** (a) Raster scan of the sample surface showing diffraction limited spots indicating the location of isolated gold nanorods. The TPL was excited with circularly polarized laser light at 760 nm, and detected at 400–600 nm. Bar length 3 μm. (b) Log-log plot confirming the two-photon nature of the excitation. (c) Normalized TPL excitation profile of four individual gold nanorods obtained from raster scans with different excitation wavelengths. The TPL intensity was obtained by integrating the photomultiplier tube voltage over the individual spots in (a). The inset shows the TPL intensity versus polarization angle of the excitation laser light.

TPL excitation profile linewidth is 70 ± 10 meV (average over 10 particles), which is significantly narrower than the linear scattering and extinction linewidths presented in Fig. 1. Additional polar plots of the excitation polarization dependent TPL intensity of three individual gold nanorods are also presented in Fig. 4c.

TPL action cross section

The TPL action cross section presented in the main text was measured on single gold nanorods (average size 45×12 nm) embedded in a thin PVA film using the formalism described by Xu and Webb.[6] For a single nanoparticle, the number of fluorescence photons detected can be expressed as[6]

$$F = g\phi\eta\sigma_2 I^2, \tag{2}$$

where g is the degree of second-order temporal coherence of the excitation source, ϕ is the collection efficiency of the setup, I is the incident photon flux (in photons/s/cm^2), $\eta\sigma_2$ is the two-photon action cross section (in cm^4 s/photon), with η the fluorescence quantum yield and σ_2 the two-photon absorption cross section. Typical values in our experiment are $g = 1.9 \times 10^5$, $\phi = 0.17$, and $I = 1 \times 10^{23}$ photons/s/cm^2. The number of detected fluorescence photons F was extracted from the peak value in the TPL excitation profile (see for example Fig. 4b) by considering the sensitivity of the photomultiplier tube. The TPL action cross section then follows from Eq. 2.

Patterning with a continuous wave laser source

Here we demonstrate multiplexed recording of patterns using a continuous wave laser source. Patterning was performed using a titanium sapphire laser source, operating in continuous wave mode. The continuous wave laser power was 80 mW at the back aperture of the 0.95 NA objective lens (60 mW in the focal plane). The exposure time on the sample was controlled by an electro-optic modulator, and was 10 ns per pixel. In Fig. 5 we show TPL raster scans of two polarization multiplexed images, recorded at 840 nm with a linear polarization (indicated by the arrows). The TPL was excited using the pulsed output from the titanium sapphire laser and was excited with the same wavelength and polarization as was used for recording.

The ability to record patterns using a continuous wave laser source significantly reduces the cost of the patterning apparatus. It enables the usage of low cost, readily available laser diodes. Combined with the transmission readout demonstrated in Supplementary Movie 1, this technique allows for straightforward integration with current drive technology.

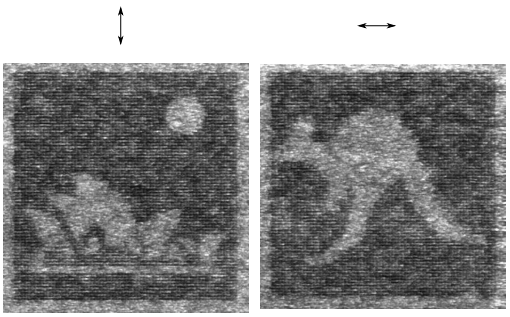

Figure 5: **Patterning with a continuous wave laser source** Polarization encoding with a continuous wave laser source of 840 nm. The laser power was 80 mW at the back aperture of the objective lens, and the exposure time per pixel was ≈10 ns. The patterns were imaged by exciting the TPL at 840 with a linear polarization and detecting the TPL at 400–600 nm. The images are 75×75 pixels and measure 100×100 μm.

Recording in ten layers

To demonstrate the feasibility of our technique for high density optical data storage on a disc, we demonstrate optical recording in ten layers spaced by 10 μm. The patterns (100×100 μm, 75×75 pixels) were recorded using single femtosecond laser pulses at 840 nm. The recording pulse energy for each layer was optimized to yield the best contrast without noticeable cross talk. As is shown by the inset in Fig. 6, we can record in the tenth layer without noticeable loss of spatial resolution and sensitivity.

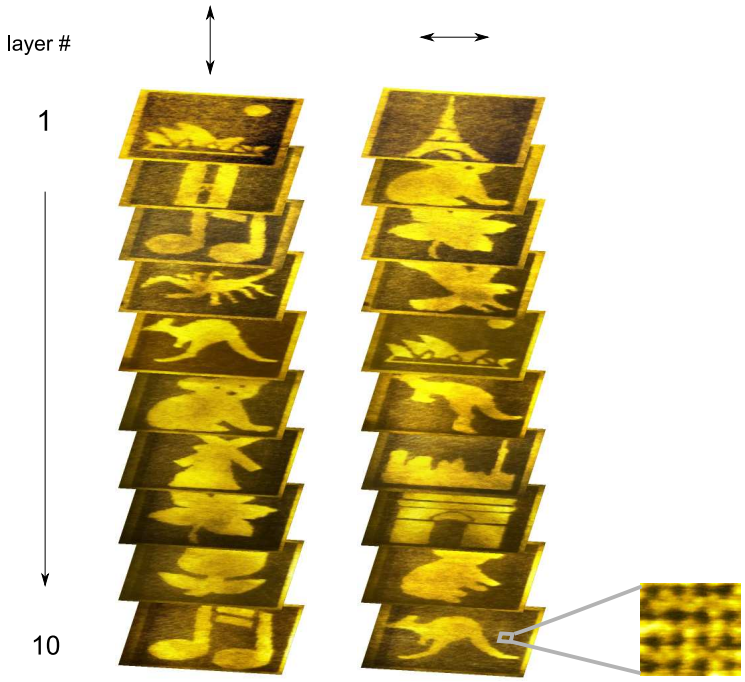

Figure 6: **Recording in many layers** Polarization multiplexed recording in ten layers spaced by 10 μm. The recorded patterns were detected by exciting the TPL at 840 nm, and detecting in the 400–600 nm window. The inset on the right shows a 6×6 μm high magnification image of the area indicated by the square.

Three-state polarization multiplexing

Here we demonstrate the multiplexed recording of three patterns in the same focal volume using three different recording laser light polarizations. The recording was done using single femtosecond laser pulses at 840 nm with a pulse energy of 160 pJ in the focal plane of the objective. Patterns were recorded using linear laser light polarizations of 0, 60, and 120 degrees relative to the laboratory frame. The recorded patterns were imaged by detecting the TPL excited with the same wavelength and polarization as was used for the recording.

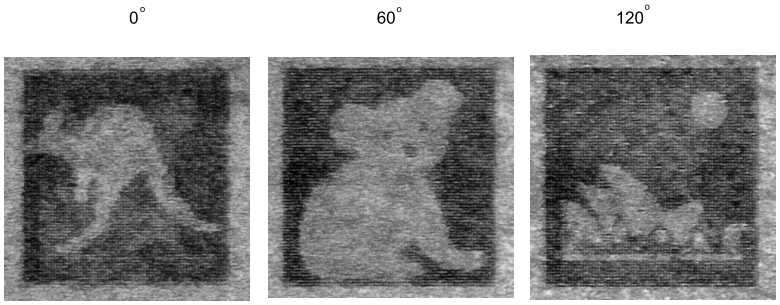

Figure 7: **Three state polarization encoding** Three state polarization encoding with single femtosecond laser pulses (λ = 840 nm, pulse energy 160 pJ.) The patterns were imaged by exciting the TPL at 840 with a linear polarization and detecting the TPL at 400–600 nm. The images are 75×75 pixels and measure 100×100 μm.

Detailed methods

Sample preparation and characterization

Gold nanorods with average aspect ratios of 2.3 ± 1, 4.3 ± 1, and 6 ± 2 were prepared using wet chemical synthesis.[7,8] After preparation, the remaining solutes were diluted by three orders of magnitude through centrifugation. The nanorod solutions were then mixed to obtain a "flat" extinction profile in the 700–1000nm wavelength range. This nanorod solution was then mixed with a 15% wt. PVA solution and spincoated on a glass coverslip. The thickness of this layer was 1 ± 0.2 μm, measured using an atomic force microscope. The approximate nanorod concentration in the film was 400 ± 50 nM, which is equivalent to a total of ≈ 200 nanorods in the focal volume of the 0.95 NA objective lens. A transparent pressure sensitive adhesive (LINTEC Co.) with a thickness of 10 ± 1 μm and a refractive index of 1.506 was laminated onto the spincoated layer. Subsequently, another recording layer was spincoated on top of the spacer layer. This process was repeated until the desired number of layers was reached.

In Fig. 8 we show the change in the extinction of the sample after subsequent spin coating of three recording layers. We observe a linear increase in extinction, indicating a consistent layer thickness and nanoparticle concentration for each layer. We measured the exact layer spacing by exciting the TPL of the gold nanorods at 760 nm and scanning the sample in the z-direction. The TPL z-scan is shown in Fig. 8b. The highest peak in the z-profile corresponds to TPL from the first recording layer. We measured z-scans on three different positions in the sample spaced by ∼5 mm (shown as three curves in Fig. 8). The layer spacing did not vary by more than 0.5 μm over this distance.

The peak TPL intensity is reduced by approximately 50 % when moving from the first to the third and deepest recording layer. This reduction in TPL intensity is caused by a combination of spherical aberration and extinction by previous recording layers. The extinction of a recording

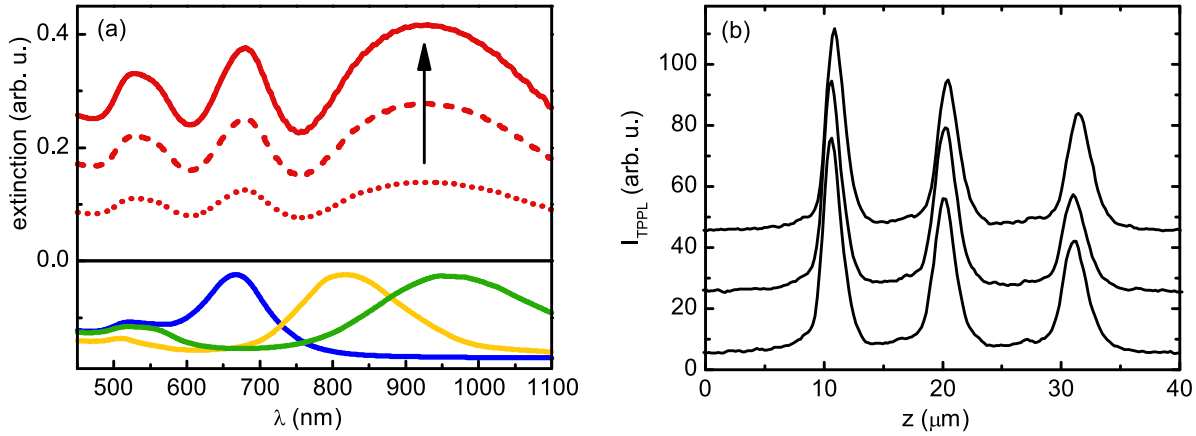

Figure 8: **Sample characterization** (a) Subsequent extinction profiles recorded of the spin coating of three recording layers. The PVA layers were doped with a broad distribution of gold nanorods. The lower panel shows the extinction spectra of the as prepared aqueous gold nanorods. (b) Depth profile of the spincoated sample. The TPL was excited at 760 nm while scanning the sample in the z-direction. The three curves represent a z-scan at three different positions in the sample, spaced by approximately 5 mm. The curves are offset for clarity.

layer is 0.07 at the excitation wavelength of 760 nm, and thus each recording layer reduces the light transmission by approximately 15%. Considering the two-photon nature of the excitation, the extinction by a recording layer will reduce the TPL intensity by ≈30% per layer, or ≈50% by two layers. This implies that the reduction in TPL intensity can be fully explained by the extinction by previous recording layers, and spherical aberration does not play a significant role for the three layers spaced by 10μm employed here.

Optical setup

Both recording and readout of the patterns was conducted in the same home built microscope. For patterning, an electro-optic modulator (ConOptics Inc., 350-160) selected single pulses on demand from the pulse train of a broadband tunable femtosecond pulse laser (SpectraPhysics Tsunami, 100 fs pulse duration, 82 MHz repetition rate, tunable between 690 and 1010 nm). In all experiments, the laser pulses were focused onto the sample through a high numerical aperture objective lens (Olympus 0.95 NA 40x, cover slip corrected). The images in the first layer were patterned using pulse energies of 0.21 nJ at 700 nm, 0.22 nJ at 840 nm, and 0.32 nJ at 980 nm (all pulse energies in the focal plane). For patterning in subsequent (deeper) layers, the pulse energy was increased by 20% per layer to compensate for extinction by previous layers.

For readout, the two-photon luminescence (TPL) of the nanorods was excited using the 82 MHz output from the femtosecond laser. The pulse train was focused on the sample through the same objective as was used for the patterning. The TPL signal was directed to a photomultiplier tube (Hamamatsu H7422P-40) and was detected in the 400–600nm wavelength range. To prevent erasure of the patterns, the pulse energy of the readout laser was almost three orders of magnitude lower than the patterning pulse energy (≈1 pJ/pulse in the focal plane, 85-100 μW average power).

References

[1] Lindfors, K.; Kalkbrenner, T.; Stoller, P.; Sandoghdar, V. *Phys. Rev. Lett.* **2004,** 93, 037401.

[2] Sönnichsen, C.; Franzl, T.; Wilk, T.; von Plessen, G.; Feldmann, J.; Wilson, O.; Mulvaney, P. *Phys. Rev. Lett.* **2002,** 88, 077402.

[3] Novo, C.; Gomez, D.; Pérez-Juste, J.; Zhang, Z. Y.; Petrova, H.; Reismann, M.; Mulvaney, P.; Hartland, G. V. *Phys. Chem. Chem. Phys.* **2006,** 8, 3540-3546.

[4] Muskens, O.L. et al. Quantitative absorption spectroscopy of a single gold nanorod. *J. Phys. Chem. C* **112**, 8917-8921 (2008).

[5] Hache, F., Ricard, D., Flytzanis, C. & Kreibig, U. The optical kerr effect in small metal particles and metal colloids: The case of gold. *Appl. Phys. A: Mater. Sci. Process.* **47**, 347-357 (1988).

[6] Xu, C. & Webb, W.W. Measurement of two-photon excitation cross sections of molecular fluorophores with data from 690 to 1050 nm. *J. Opt. Soc. Amer. B* **13**, 481-491 (1996).

[7] Nikoobakht, B. & El-Sayed, M.A. Preparation and growth mechanism of gold nanorods (NRs) using seed-mediated growth method. *Chem. Mater.* **15**, 1957-1962 (2003).

[8] Zijlstra, P., Bullen, C., Chon, J.W.M. & Gu, M. High-temperature seedless synthesis of gold nanorods. *J. Phys. Chem. B* **110**, 19315-19318 (2006).